Eigenvalue Approach to the Efficient Determination of the Hybrid and Complex Spectrum of Inhomogeneous, Closed Waveguide

Tullio Rozzi, *Fellow, IEEE,* Luca Pierantoni, and Marco Farina

***Abstract*— Many hybrid modes are required in computing the fields scattered from discontinuities in structures such as finline, coplanar waveguide, or microstrip. The authors present a new analytical method based on an eigenvalue formulation of the generalized telegrapher's equations discretized by using the modes at cutoff as an expanding set. This approach produces a compact theoretical model while providing at the same time an effective algorithm for finding the characteristics of many modes, including their below cutoff and complex behavior. The theoretical approach gives some direct insights about the appearance of complex modes. Due to the explicit formulation of the eigenvalue equation for the complex propagation constant, the proposed method overcomes some of the typical drawbacks of the currently used algorithms, such as the limited numerical accuracy and efficiency, the numerical degeneracy and appearance of spurious solutions, the inability to trace the characteristics of degenerate modes. Numerical results for ordinary and complex propagation in finline show excellent agreement with existing data.**

I. Introduction

Apart from numerical techniques, the semi-analytic determination of the hybrid modes of common lossless reciprocal metal-dielectric guides such as finline and microstrip is currently based on transverse resonance in its spectral domain approach (SDA) [1] or transverse resonance diffraction (TRD) version [2]. A coupled transmission line approach, obtained in terms of the modes of the empty guide is used in the literature as a tool appropriate for theoretical investigation, but unsuited for numerical implementation [3], [4] due to the very large number of coupled transverse electric/transverse magnetic (TE/TM) lines resulting from this discretization of the guide.

Starting from the differential equations governing the propagation of the transverse fields along the guide [5], however, it is possible to formulate and discretize a direct eigenvalue problem in terms of a new set of frequency-independent real vector fields that *implicitly* satisfy all boundary and edge conditions of the real problem, coinciding with the exact hybrid fields at the modal cutoffs. The formal completeness of the new expanding functions set is guaranteed by the fact that they constitute the eigenfunctions of the transverse wave equation (5). Orthonormality of the expanding set is not actually required in the discretization process.

Manuscript received October 17, 1995; revised November 21, 1996.

The authors are with Dipartimento di Elettronica ed Automatica, Università degli Studi di Ancona, 60131 Ancona, Italy.

Publisher Item Identifier S 0018-9480(97)01725-0.

As will be described briefly, the new expanding functions feature some very remarkable properties that greatly simplify the analytical model as well as the discretization process. Moreover, their use produces a compact and numerically effective algorithm for tracing the dispersion characteristics of numerous modes of the spectrum, as required, e.g., in abrupt discontinuity problems. The modes resulting from this method are not automatically orthonormal, but if required, they be made so by application of the classical Gram–Schmidt algorithm.

Numerical examples of ordinary and complex propagation are provided for the case of unilateral finline with infinitely thin metallization.

It is noted that although finite thickness is currently accounted for in recent works on this subject [9], [10], because of its singular edge condition, the thin case actually poses the hardest convergence test of the field expansion.

II. Theory

The authors start with the field equations governing the propagation of the transverse fields along the guide, in absence of sources as in [5]. These are

$$\begin{aligned}\frac{\partial \mathbf{E}_t}{\partial z} &= -j\omega\mu\left(\bar{\bar{\mathbf{I}}} + \nabla_t \frac{1}{k^2}\nabla_t\right)\cdot(\mathbf{H}_t \times \hat{\mathbf{z}}) \\ \frac{\partial \mathbf{H}_t}{\partial z} &= -j\omega\varepsilon_r\varepsilon_0\left(\bar{\bar{\mathbf{I}}} + \nabla_t \frac{1}{k^2}\nabla_t\right)\cdot(\hat{\mathbf{z}} \times \mathbf{E}_t)\end{aligned} \tag{1}$$

where $\mathbf{E}_t = \mathbf{e}_t e^{-\gamma Z}$, $\mathbf{H}_t = \mathbf{h}_t e^{-\gamma Z}$ are the transverse components of the hybrid field, $\bar{\bar{\mathbf{I}}}$ is the dyadic identity, $k^2 = \varepsilon_r k_0^2$, k_0 is the free-space wavenumber; $\mathbf{e}_t$, $\mathbf{h}_t$ each contain both longitudinal-section (LSE)/electric–magnetic (LSM) components which separate at cutoff [6], where $\gamma = 0$.

If the authors write $\mathbf{e}_t = \mathbf{e}_t^{\mathrm{LSE}} + \mathbf{e}_t^{\mathrm{LSM}}$, $\mathbf{h}_t = \mathbf{h}_t^{\mathrm{LSE}} + \mathbf{h}_t^{\mathrm{LSM}}$, the following properties of these components can also be proved at cutoff (see the Appendix):

$$\begin{aligned}\mathbf{e}_t &= \mathbf{e}_t^{\mathrm{LSM}} = (e_x,\, e_y) \\ e_x &= \partial_x\partial_y\Psi_e \\ e_y &= (\varepsilon_r k_t^2 + \partial_y^2)\Psi_e \\ e_z^{\mathrm{LSM}} &= 0\end{aligned} \tag{2a}$$

$$\begin{aligned}\mathbf{h}_t &= \mathbf{h}_t^{\mathrm{LSE}} = (h_x,\, h_y) \\ h_x &= \partial_x\partial_y\Psi_h \\ h_y &= (\varepsilon_r k_t^2 + \partial_y^2)\Psi_h \\ h_z^{\mathrm{LSE}} &= 0\end{aligned} \tag{2b}$$

$$(\partial_x^2+\partial_y^2+\varepsilon_r k_{te,h}^2)\Psi_{e,h}=0$$
$$\nabla_t\cdot\mathbf{e}^{\mathrm{LSM}}=0$$
$$\nabla_t\cdot\mathbf{h}^{\mathrm{LSE}}=0 \tag{3}$$

where $\Psi_e\Psi_h$ are the electric/magnetic Hertzian potentials, $k_{te,h}$ the cutoff wavenumbers of the LSE/LSM parts of the field, respectively; from Lorentz's theorem, the authors have, for the LSE/LSM components of two distinct modes (m, n):

$$\iint_S \varepsilon\mathbf{e}_{t_n}\cdot\mathbf{e}_{t_m}\,dS=\mu_0\iint_S h_{z_n}\cdot h_{z_m}\,dS \tag{4a}$$
$$\iint_S \varepsilon e_{z_n}\cdot e_{z_m}\,dS=\mu_0\iint_S \mathbf{h}_{t_n}\cdot\mathbf{h}_{t_m}\,dS. \tag{4b}$$

Moreover, it can be shown that the LSE/LSM components at cutoff are solutions of the following transverse eigenvalue equations and, consequently, they form a complete set

$$\nabla_t\left\{\frac{1}{k^2}\nabla_t\cdot(\mathbf{h}_t^{\mathrm{LSE}}\times\hat{\mathbf{z}})\right\}=-\frac{k_{te}^2}{k_0^2}\,\mathbf{h}_t^{\mathrm{LSE}}\times\hat{\mathbf{z}} \tag{5a}$$
$$\nabla_t\left\{\frac{1}{k^2}\nabla_t\cdot(\hat{\mathbf{z}}\times\mathbf{e}_t^{\mathrm{LSM}})\right\}=-\frac{k_{th}^2}{k_0^2}\,\hat{\mathbf{z}}\times\mathbf{e}_t^{\mathrm{LSM}}. \tag{5b}$$

On account of these noteworthy properties of the LSE/LSM modal components at cutoff, *the authors select these as an expanding set for the transverse fields*: in this way all boundary and edge conditions are implicitly enforced and satisfied; in particular, the authors expand the transverse fields of a hybrid mode as

$$\mathbf{E}_t(\omega)=\sum_{k\in\mathrm{LSE}}V_k^h(\omega)(\mathbf{h}_{t_k}\times\mathbf{z})+\sum_{k\in\mathrm{LSM}}V_k^e(\omega)\mathbf{e}_{t_k} \tag{6a}$$
$$\mathbf{H}_t(\omega)=\sum_{k\in\mathrm{LSE}}I_k^h(\omega)\mathbf{h}_{t_k}+\sum_{k\in\mathrm{LSM}}I_k^e(\omega)(\mathbf{z}\times\mathbf{e}_{t_k}). \tag{6b}$$

By substituting (6) in (1) and exploiting the above properties (3)–(5), the authors will recover a particularly simple, discretized version of (1).

As a starting point the authors insert the transverse fields $\mathbf{E}_t$ and $\mathbf{H}_t$ (6) in (1), obtaining

$$\begin{aligned}&-\gamma\left[\sum_k V_k^h(\omega)\,(\mathbf{h}_{t_k}\times\hat{z})+\sum_k V_k^e(\omega)\mathbf{e}_{t_k}\right]\\&=-j\omega\mu\left[\sum_k I_k^h(\omega)\,(\mathbf{h}_{t_k}\times\hat{z})+\sum_k I_k^e(\omega)\,\mathbf{e}_{t_k}\right]\\&\quad+j\omega\mu\sum_k I_k^h(\omega)\left[\frac{k_{th}^2}{k^2}\,(\mathbf{h}_{t_k}\times\hat{z})\right]\end{aligned} \tag{7a}$$

$$\begin{aligned}&-\gamma\left[\sum_k I_k^h(\omega)\,\mathbf{h}_{t_k}+\sum_k I_k^e(\omega)\,(\hat{z}\times\mathbf{e}_{t_k})\right]\\&=-j\omega\varepsilon\left[\sum_k V_k^h(\omega)\,\mathbf{h}_{t_k}+\sum_k V_k^e(\omega)\,(\hat{z}\times\mathbf{e}_{t_k})\right]\\&\quad+j\omega\varepsilon\sum_k V_k^e\left[\frac{k_{te}^2}{k^2}\,(\hat{z}\times\mathbf{e}_{t_k})\right].\end{aligned} \tag{7b}$$

Now the authors form the scalar product between $(\mathbf{h}_{t_k}^*\times\hat{z})$, $\mathbf{e}_{tk}^*$, $(k=1,\cdots,n)$ and (7a) and (7b) $\times\hat{\mathbf{z}}$, respectively, yielding, after integration over the cross section S:

$$\gamma\tilde{\mathbf{A}}\begin{pmatrix}\mathbf{V}^h\\\mathbf{V}^e\end{pmatrix}=\mu_0\left[s\tilde{\mathbf{A}}+\frac{1}{s}\,\tilde{\mathbf{A}}\begin{pmatrix}\Omega_h&0\\0&0\end{pmatrix}\right]\begin{pmatrix}\mathbf{I}^h\\\mathbf{I}^e\end{pmatrix} \tag{8a}$$
$$\gamma\tilde{\mathbf{A}}+\begin{pmatrix}\mathbf{I}^h\\\mathbf{I}^e\end{pmatrix}=\left[s\tilde{\mathbf{C}}+\frac{1}{s}\tilde{\mathbf{C}}\begin{pmatrix}0&0\\0&\Omega_e\end{pmatrix}\right]\begin{pmatrix}\mathbf{V}^h\\\mathbf{V}^e\end{pmatrix}. \tag{8b}$$

Equations (8a) and (8b) form the sought compact version of (1), being $s=j\omega$ and

$$\mathbf{V}^h(\omega)=\begin{pmatrix}V_1^h\\V_2^h\\\vdots\end{pmatrix}$$
$$\mathbf{V}^e(\omega)=\begin{pmatrix}V_1^e\\V_2^e\\\vdots\end{pmatrix}$$
$$\mathbf{I}^h(\omega)=\begin{pmatrix}I_1^h\\I_2^h\\\vdots\end{pmatrix}$$
$$\mathbf{I}^e(\omega)=\begin{pmatrix}I_1^e\\I_2^e\\\vdots\end{pmatrix} \tag{9}$$

being the vectors of the LSE/LSM amplitudes appearing in (6).

In (8a) and (8b) the authors introduced

$$\Omega_h=\mathrm{diag}\,(k_{t_{h_1}}^2,\cdots,k_{t_{h_n}}^2)$$
$$\Omega_e=\mathrm{diag}\,(k_{t_{e_1}}^2,\cdots,k_{t_{e_n}}^2)$$

$\tilde{\mathbf{A}}$ is the real matrix formed by the "overlapping" of the real expanding functions, $\tilde{\mathbf{A}}^+(=\tilde{\mathbf{A}}^t)$ its hermitian conjugate, $\tilde{\mathbf{C}}$ describes the same overlapping weighted by the dielectric constant ε. Both these matrices are block-partitioned and of the Hermitian type:

$$\begin{aligned}\tilde{\mathbf{A}}&=\begin{bmatrix}\mathbf{A}_{11}&\mathbf{A}_{12}\\\mathbf{A}_{21}&\mathbf{A}_{22}\end{bmatrix}\mathbf{A}_{21}\\&=\mathbf{A}_{12}^+\\\mathbf{A}_{11}^{m,p}&=\iint_S\mathbf{h}_{t_m}^*\cdot\mathbf{h}_{t_p}\,dS\\\mathbf{A}_{12}^{m,p}&=\iint_S(\mathbf{h}_{t_m}^*\times\hat{\mathbf{z}})\cdot\mathbf{e}_{t_p}\,dS\\\mathbf{A}_{22}^{m,p}&=\iint_S\mathbf{e}_{t_m}^*\cdot\mathbf{e}_{t_p}\,dS\end{aligned} \tag{10a}$$

$$\begin{aligned}\hat{\mathbf{C}}&=\begin{bmatrix}\mathbf{C}_{11}&\mathbf{C}_{12}\\\mathbf{C}_{21}&\mathbf{C}_{22}\end{bmatrix}\mathbf{C}_{21}\\&=\mathbf{C}_{12}^+\\\mathbf{C}_{11}^{m,p}&=\iint_S\varepsilon\mathbf{h}_{t_m}^*\cdot\mathbf{h}_{t_p}\,dS\\\mathbf{C}_{12}^{m,p}&=\iint_S\varepsilon(\mathbf{h}_{t_m}^*\times\hat{\mathbf{z}})\cdot\mathbf{e}_{t_p}\,dS\\\mathbf{C}_{22}^{m,p}&=\iint_S\varepsilon\mathbf{e}_{t_m}^*\cdot\mathbf{e}_{t_p}\,dS,\qquad m,p=1,\cdots,n.\end{aligned} \tag{10b}$$

Since the fields are, in fact, real, the authors have $\tilde{\mathbf{A}} = \tilde{\mathbf{A}}^{+}$; $\tilde{\mathbf{C}} = \tilde{\mathbf{C}}^{+}$.

The $\Omega_{h,e}$ are diagonal matrices formed by the squares of the LSE/LSM cutoff frequencies, respectively. It is also noted that at cutoff ($\gamma = 0$), the right-hand side (RHS) of (8) become eigenvalue equations for the cutoff frequencies.

It is noted that the expansion functions individually satisfy boundary and edge conditions on strips/apertures, being the exact solutions at cutoff. In fact, a single term expansion in (6) is very accurate for an ordinary mode even well above cutoff.

Each of the two systems (8a) and (8b) is constituted by $2n$-linear equations in $4n$-unknown expanding coefficients $V_1^h, \cdots, V_n^h, V_1^e, \cdots, V_n^e, I_1^h, \cdots, I_n^h, I_1^e, \cdots, I_n^e$; therefore (8a) and (8b) can be combined in order to form a single system characterized by $2n$-equations in $2n$-unknown coefficients $V_1^h, \cdots, V_n^h, V_1^e, \cdots, V_n^e$, (or $I_1^h, \cdots, I_n^h, I_1^e, \cdots, I_n^e$); its determinant is a polynomial equation for the square of the complex propagation constant, γ^2.

Firstly, the authors premultiply (6a) and (6b) by $\tilde{\mathbf{A}}^{-1}$ (the inverse of $\tilde{\mathbf{A}}$, assumed nonsingular) and divide both members by γ obtaining

$$\begin{bmatrix} \mathbf{V}^h \\ \mathbf{V}^e \end{bmatrix} = \frac{\mu}{\gamma}\left[s\bar{\bar{\mathbf{I}}} + \frac{1}{s}\begin{pmatrix} \Omega_h & 0 \\ 0 & 0 \end{pmatrix}\right]\begin{bmatrix} \mathbf{I}^h \\ \mathbf{I}^e \end{bmatrix}. \tag{11}$$

Substituting $\left[\begin{smallmatrix} \mathbf{V}^h \\ \mathbf{V}^e \end{smallmatrix}\right]$ from the above equation in (8b) yields

$$\gamma\tilde{\mathbf{A}}^{+}\begin{bmatrix} \mathbf{I}^h \\ \mathbf{I}^e \end{bmatrix} = \frac{\mu}{\gamma}\left[s\tilde{\mathbf{C}} + \frac{1}{s}\tilde{\mathbf{C}}\begin{pmatrix} 0 & 0 \\ 0 & \Omega_e \end{pmatrix}\right] \cdot \left[s\bar{\bar{\mathbf{I}}} + \frac{1}{s}\begin{pmatrix} \Omega_h & 0 \\ 0 & 0 \end{pmatrix}\right]\begin{bmatrix} \mathbf{I}^h \\ \mathbf{I}^e \end{bmatrix}$$

hence, for $s = j\omega$:

$$\gamma^2\tilde{\mathbf{A}}\begin{bmatrix} \mathbf{I}^h \\ \mathbf{I}^e \end{bmatrix} = -\omega^2\mu\tilde{\mathbf{C}}\tilde{\Gamma}\begin{bmatrix} \mathbf{I}^h \\ \mathbf{I}^e \end{bmatrix} \tag{12}$$

where

$$\tilde{\Gamma} = \begin{bmatrix} \Gamma_h' & 0 \\ 0 & \Gamma_e' \end{bmatrix}$$

$$\Gamma_{h,e} = \operatorname{diag}\left(1 - \frac{\omega_{t_{k_{h,e}}}^2}{\omega^2}\right)$$

that is, $\tilde{\Gamma}$ is a diagonal matrix with elements of the type: $1 - \omega_{t_{k_{e,h}}}^2/\omega^2$, $\omega_{t_{k_{e,h}}}$ being the cutoff frequency of the LSM or LSE component in (6a) and (6b). In (12), the authors took into account that $\tilde{\mathbf{A}}^{+} = \tilde{\mathbf{A}}$ (the field at cutoff being pure real). Equation (12) can be rewritten as

$$\frac{\gamma^2}{k_0^2}\tilde{\mathbf{A}}\begin{bmatrix} \mathbf{I}^h \\ \mathbf{I}^e \end{bmatrix} = -\frac{1}{\varepsilon_0}\tilde{\mathbf{C}}\tilde{\Gamma}\begin{bmatrix} \mathbf{I}^h \\ \mathbf{I}^e \end{bmatrix}. \tag{13}$$

Consequently, the authors are left with just a generalized eigenvalue problem for γ^2.

Once the frequency is fixed, each eigenvalue $\gamma^2(\omega)$ yields the corresponding eigenvector $\mathbf{I} = \left[\begin{smallmatrix} \mathbf{I}^h \\ \mathbf{I}^e \end{smallmatrix}\right]$, which, in turn, gives the transverse modal magnetic field $\mathbf{H}_t$ in (6b). The other eigenvector $\mathbf{V} = \left[\begin{smallmatrix} \mathbf{V}^h \\ \mathbf{V}^e \end{smallmatrix}\right]$, producing the TE field $\mathbf{E}_t$ in (6a), can be easily derived from (8a). The longitudinal components $\mathbf{E}_z$, $\mathbf{H}_z$ are evaluated as in [4]:

$$H_z = \frac{\nabla_t \cdot (\mathbf{z} \times \mathbf{E}_t)}{j\omega\mu}$$

$$E_z = \frac{\nabla_t \cdot (\mathbf{H}_t \times \mathbf{z})}{j\omega\varepsilon}.$$

It is particularly convenient to deal with the *explicit* eigenvalue (12), for, in this case, the eigenvalues $\gamma^2(\omega)$ are obtained in a direct manner through the solution of (13), by means of any one of the many reliable and compact algorithms that are currently available.

On the other hand, in the standard Transverse Resonance Methods, the construction of the modal curves is based on the solution of an *implicit* eigenvalue problem in a more general sense, that is, of the type:

$$\tilde{\mathbf{Z}}[\omega, \gamma(\omega)]\mathbf{x} = 0 \tag{14a}$$

where $\tilde{\mathbf{Z}}$ is the transverse immittance of the guide and the dispersion curves are evaluated by imposing the condition:

$$f[\gamma(\omega)] = \det\{\tilde{\mathbf{Z}}[\omega, \gamma(\omega)]\} = 0 \tag{14b}$$

where the difficulty is posed by the search of the complex zeros of the rapidly varying function $f[\gamma(\omega)]$.

Another difficulty is usually constituted by the exact construction of the modal characteristics, that is the correct attribution to the kth mode of the corresponding $\beta_k(\omega)$ curve without overlapping with other curves. In synthesis, the present method consists of three steps.

1) Search of the cutoff frequencies and their related transverse vector fields components $\mathbf{e}_t, \mathbf{h}_t$ to be used as expanding eigenfunctions in (6a) and (6b).
2) Solution of the eigenvalue equation (13) and determination of the corresponding eigenvector $\mathbf{V}(\omega)$, $\mathbf{I}(\omega)$.
3) Construction of the dispersion characteristics and of the modal field for every mode under investigation.

The second step is the kernel of the present method which is applicable to any type of lossless closed waveguide, being able to describe any type of propagating mode in the structure, that is, ordinary modes (apart from the TEM mode) as well as complex modes, as illustrated in the next paragraph.

Comparing the explicit eigenvalue equation (13) and the standard dispersion equation (14b) some of the most attractive features of the former become evident.

a) Cutoff fields and frequencies are easier to compute then ordinary points: once they have been computed by means of any technique, e.g., the TRD method, the dispersion curves are found by finding the eigenvalues of (13): this is a simple task and it takes only a negligible time with respect to using (14b). Consequently, our algorithm becomes increasingly advantageous and effective as the frequency band to be scanned increases.

b) Due to the particular choice of the discretizing functions, just two expanding functions are normally involved from an ordinary mode, one LSE, the other LSM, so that matrix dimensions are very small and numerical accuracy is inherently high. On the other hand, techniques that rely on equations such as (14), have to handle cumbersome matrices with nearly vanishing determinants, posing the well known problems of numerical accuracy and numerical degeneracy (spurious solutions, crossing of characteristics). This is also true for the determination of fields: the frequency dependence of the field is contained in the coefficient V_k and I_k and (6) allows this dependence to be computed at all frequencies very simply.

c) At cutoff the modes are pure LSE or LSM; by using one mode LSE and one LSM as expanding functions, the authors can trace two hybrid characteristics, originating from the two cutoff modes. By repeating this procedure, a number of modal characteristics can be traced; the existence of degenerate modes does not pose any particular problem. When solving (14), instead, it often happens that when following the zeros of the determinant, the numerical solution skips from one characteristic to another, particularly when dealing with degenerate modes. Indeed, our approach allows to correctly trace the characteristic curves for many modes, overcoming the problems associated with degenerate modes and avoiding the appearance of spurious solutions.

III. Complex Modes

The main features of complex modes are as follows:

1) they have complex propagation constants despite the lossless nature of the structure;
2) a single complex mode carries no complex power, two complex waves form a pair that is not orthogonal with respect to cross power and consequently a pair as a whole behaves as an ordinary mode below cutoff carrying purely reactive power. Now let us consider equation (8a) and form the scalar product

$$\mathbf{I}^{+}\tilde{\mathbf{A}}\mathbf{V} = \mathbf{I}^{+}\tilde{\mathbf{Q}}\mathbf{I} \tag{15}$$

where the authors have set:

$$\tilde{\mathbf{Q}} = \frac{\mu_0}{\gamma}\left[s\tilde{\mathbf{A}} + \frac{1}{s}\tilde{\mathbf{A}}\begin{pmatrix}\Omega_h & 0\\ 0 & 0\end{pmatrix}\right].$$

From a physical point of view, (15) represents just the complex power carried by a single mode, that is

$$\begin{aligned} P &= \iint_S (\mathbf{E}\times\mathbf{H}^{*})\cdot\mathbf{dS}\\ &= \mathbf{I}^{+}\tilde{\mathbf{A}}\mathbf{V}\\ &= \mathbf{I}^{+}\tilde{\mathbf{Q}}\mathbf{I} \end{aligned} \tag{16}$$

being $\mathbf{V} = \mathbf{V}(\omega)$, $\mathbf{I} = \mathbf{I}(\omega)$ [$\mathbf{I}^{+}(\omega)$ is its Hermitian conjugate], the eigenvectors corresponding to a γ-eigenvalue.

In the light of (15), (16) and taking into account property 2) above, the authors derive necessary and sufficient conditions in order to obtain complex modes:

$$\begin{aligned} P_1 &= \iint_S (\mathbf{E}_1\times\mathbf{H}_1^{*})\cdot\mathbf{dS}\\ &= \mathbf{I}_1^{+}\tilde{\mathbf{A}}\mathbf{V}_1\\ &= \mathbf{I}_1^{+}\tilde{\mathbf{Q}}\mathbf{I}_1\\ &= 0\\ P_2 &= \iint_S (\mathbf{E}_2\times\mathbf{H}_2^{*})\cdot\mathbf{dS}\\ &= \mathbf{I}_2^{+}\tilde{\mathbf{A}}\mathbf{V}_2\\ &= \mathbf{I}_2^{+}\tilde{\mathbf{Q}}\mathbf{I}_2\\ &= 0. \end{aligned} \tag{17}$$

In the bilinear forms (17), $\mathbf{I}_1(\omega)$, $\mathbf{V}_1(\omega)$ are the eigenvectors of (8) corresponding to the complex eigenvalue γ; $\mathbf{I}_2(\omega)$, $\mathbf{V}_2(\omega)$ those corresponding to the complex conjugate eigenvalue γ^{*}. P_1 represents the power carried by the first mode [$\mathbf{I}_1(\omega)$, $\mathbf{V}_1(\omega)$] when the authors consider it individually, i.e., not coupled with the second one characterized by $\mathbf{I}_2(\omega)$, $\mathbf{V}_2(\omega)$. Dually, P_2 represents the power carried by $\mathbf{I}_2(\omega)$, $\mathbf{V}_2(\omega)$, when the authors consider it on its own, i.e., not coupled with $\mathbf{I}_1(\omega)$, $\mathbf{V}_1(\omega)$.

On the other hand, the complex power carried by a pair of complex modes, that is when both $\mathbf{I}_1$, $\mathbf{V}_1$ and $\mathbf{I}_2$, $\mathbf{V}_2$ are coupled to each other, must be nonvanishing, that is

$$\begin{aligned} P_{12} &= \iint_S (\mathbf{E}_1\times\mathbf{H}_2^{*})\cdot\mathbf{dS}\\ &= \mathbf{I}_2^{+}\tilde{\mathbf{A}}\mathbf{V}_1\\ &= \mathbf{I}_2^{+}\tilde{\mathbf{Q}}\mathbf{I}_1\\ &= p\\ P_{21} &= \iint_S (\mathbf{E}_2\times\mathbf{H}_1^{*})\cdot\mathbf{dS}\\ &= \mathbf{I}_1^{+}\tilde{\mathbf{A}}\mathbf{V}_2\\ &= \mathbf{I}_1^{+}\tilde{\mathbf{Q}}\mathbf{I}_2\\ &= -p^{*}. \end{aligned} \tag{18}$$

Since the sum of P_{12} and P_{21} produces just reactive power, a pair of complex modes behaves as a mode below cutoff carrying purely reactive power; they form a pair not orthogonal over the cross section.

In general, in order to satisfy (17), the $\tilde{\mathbf{A}}$ matrix must to be indefinite; this result is in accordance with that reported in [8].

IV. Results

A. The Unilateral Finline

The authors now compare the results of the new approach with existing ones in the case of finline with thin metallization, as in this case the inverse square root edge condition poses the hardest convergence test of the fields.

As discussed in the previous section, the present method requires an independent initial calculation and storage of modal cutoffs and of the LSE/LSM components of the field

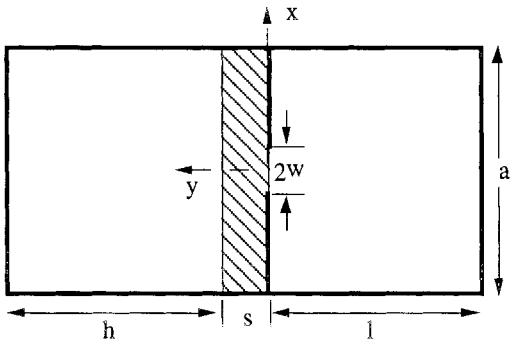

Fig. 1. Unilateral finline cross section; $a = 10.16$ mm, $l = h + s = 11.43$ mm, $s = 0.254$ mm, $2w = 0.2a$, $\varepsilon_r = 2.2$.

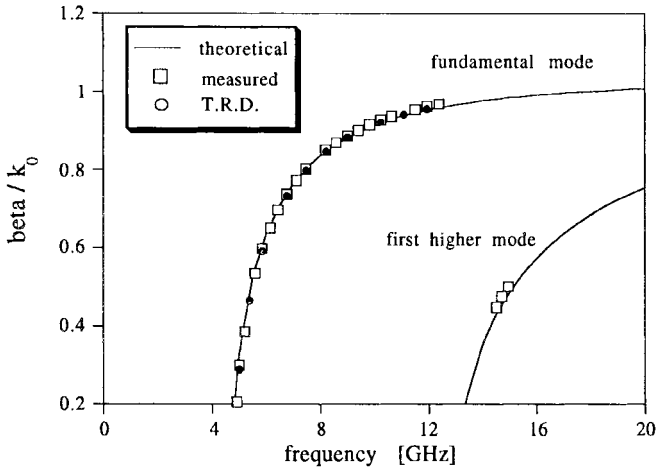

Fig. 2. Comparison between present theoretical data, TRD results and experimental values of the dispersion curves [6].

distributions at cutoff to be used in (6) and (13). The propagation constant being zero, this is a quick process, that can be accomplished once by using any classical technique, e.g., TRD as employed in [2] or [6]. It is noted that the precision required in the cutoff frequencies is an order of magnitude higher than for the cutoff fields, the latter not constituting particularly sensitive data.

Also the authors have to compute only once the frequency independent matrices $\tilde{\mathbf{A}}$, $\tilde{\mathbf{C}}$ appearing in (8), (13) from the stored fields values at cutoff. After this point, the solution of (8), (13) and the tracing of dispersion characteristics is a virtually analytical task, for the prudent choice of the expanding set ensures *a priori* satisfaction of all boundary and edge conditions so that the dimensions of matrices $\tilde{\mathbf{A}}$, $\tilde{\mathbf{C}}$ are very limited indeed; just two terms, one LSM, one LSE (overall system dimensions 4×4) are sufficient to describe even a complex mode.

B. Ordinary Modes

Fig. 1 shows the finline cross section adopted in the numerical examples of Figs. 2–4; the geometrical characteristics and cutoff frequencies computed by TRD for the first 15 modes are shown in Table I.

In Fig. 2, the authors compare the propagation constants computed by this approach with experimental values of [6]

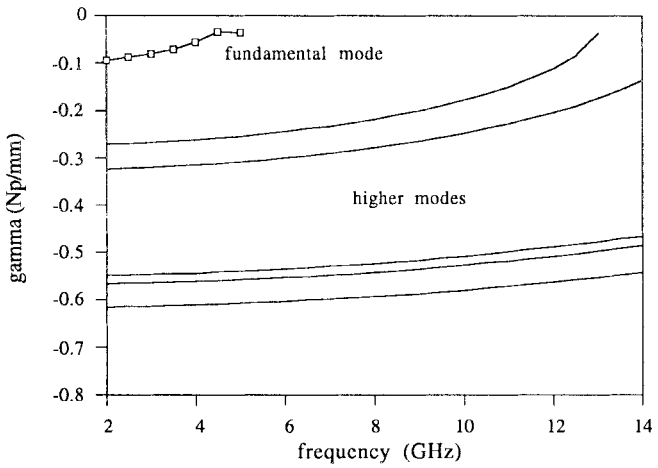

Fig. 3. Attenuation constants for the first six modes.

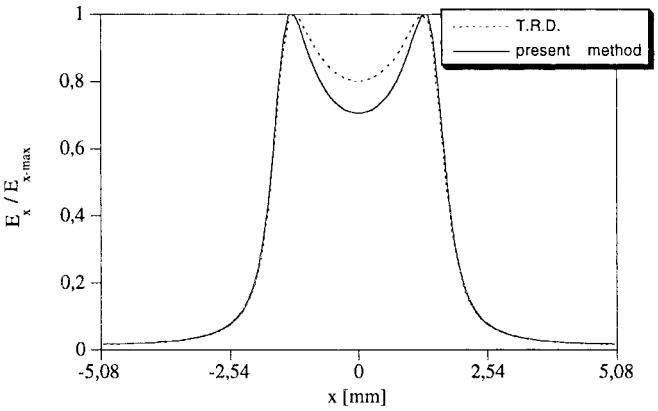

(a)

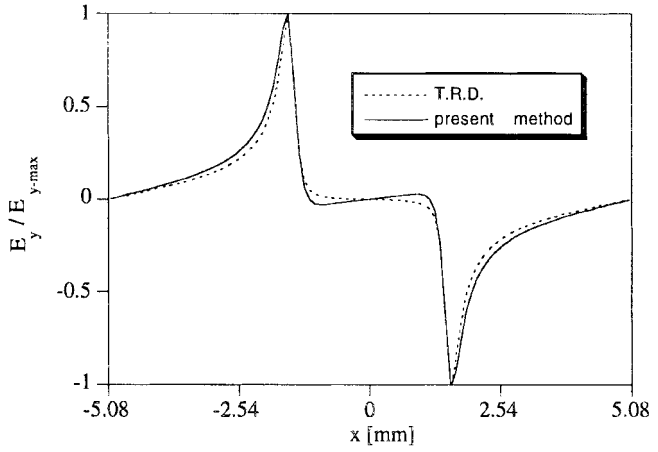

(b)

Fig. 4. (a) $E_x(x, y_1)$ field behavior for the finline of Fig. 1, with $y_1 = 0.1143$ mm (continuous line: present analysis; dashed lines: TRD [6]). (b) $E_y(x, y_1)$ field behavior for finline in Fig. 1, with $y_1 = 0.1143$ mm (continuous line: present analysis; dashed lines: TRD [6]).

for the first two modes of the above finline; one notes that theoretical results of [6] are indistinguishable from the present ones. The running time required for this computation is greatly reduced with respect to the TRD approach: this is mainly due to the explicit form of the eigenvalue equation, not requiring an iterative algorithm; moreover the above feature is responsible

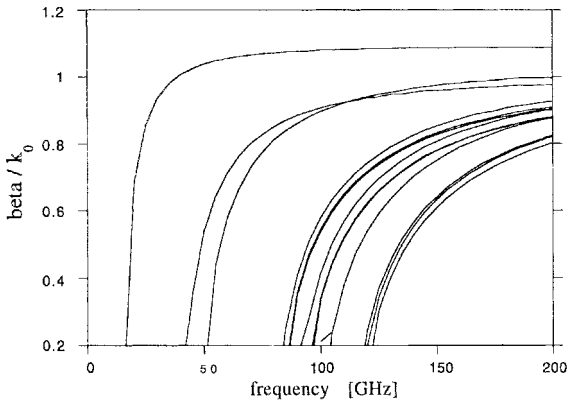

Fig. 5. Dispersion curves for the finline of Table II, with $2w = 1.1$ mm.

TABLE I
MODAL CUTOFF FREQUENCIES OF THE FIRST 15 MODES FOR THE FINLINE OF FIG. 1

order	Cut-off frequency (GHz)	type
1	5.1681	LSM
2	13.144	LSM
3	16.005	LSM
4	26.224	LSM
5	26.227	LSM
6	27.251	LSM
7	29.410	LSM
8	30.240	LSE
9	30.240	LSM
10	31.956	LSE
11	32.290	LSE
12	34.516	LSE
13	34.517	LSM
14	39.206	LSE
15	39.269	LSM

for a great improvement in all cases where modal degeneracy occurs. Some examples of this kind are depicted in Fig. 5.

In Fig. 3, the authors show the attenuation constants computed by this approach, for the first six modes, whereas the authors report in Fig. 4(a) the $E_x(x, y)$ field behavior, the main field component, at the point $y = 0.1143$ mm that falls in the dielectric, but very close to the fins; this location is significant, since the EM field decays very quickly away from the fins; Fig. 4(b) shows the $E_y(x, y)$ field behavior at the same point: in both cases results are compared with those computed with the TRD method and good agreement is obtained. These results validate our approach.

C. Complex Modes

Previous works have demonstrated that finline can support complex waves [7]–[10].

If the unperturbed guide, i.e., the rectangular metallic box loaded with a dielectric slab without the fins, allows *degenerate* modes, one of the LSE-type, the other of the LSM-type, by introducing the fins, it is possible to produce complex modes, even if the permittivity of the dielectric slab is low.

Physically, the metallic insert is a source of diffraction and it causes energy coupling between the two degenerate LSE/LSM modes: this fact is a prerequisite for the appearance of complex waves. Hence the ability of the present approach of effectively treating degenerate modes is a very convenient feature for investigating complex modes.

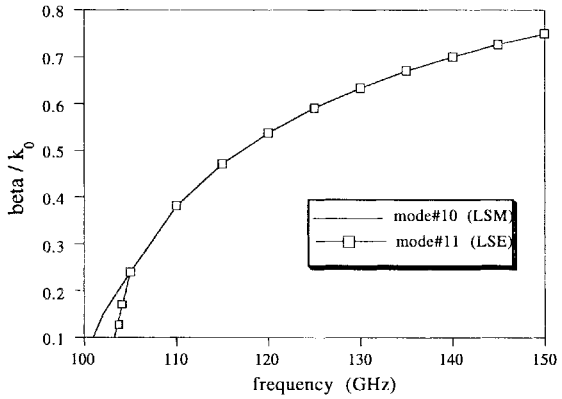

Fig. 6. Dispersion curves for the 10th (LSM) and 11th (LSE) modes of the finline of Table II ($2w = 1.1$ mm, the same of Fig. 4).

TABLE II
GEOMETRY AND PERMITTIVITY DEFINING THE SECOND EXAMPLE OF FINLINE

a	3.556 mm
$s + h$	3.556 mm
s	0.254 mm
l	3.556 mm
ε_r	2.22

TABLE III
CUTOFF FREQUENCIES OF THE FIRST 15 MODES FOR THE FINLINE OF TABLE II

order	F_c (GHz) $2w = 1.1$ mm	F_c (GHz) $2w = 1.3$ mm	type
1	15.561	16.256	LSM
2	42.123	42.123	LSM
3	49.699	50.756	LSM
4	82.397	82.429	LSM
5	84.029	84.042	LSM
6	84.370	84.435	LSM
7	91.281	88.673	LSM
8	93.947	93.760	LSE
9	94.216	94.206	LSE
10	102.097	102.609	LSM
11	102.100	102.609	LSE
12	116.428	116.428	LSE
13	117.650	117.656	LSE
14	119.055	118.998	LSM
15	119.055	121.593	LSE

To this purpose, the authors refer to another finline, whose geometrical parameters and some significant cutoff frequencies for the first 15 modes are shown in Tables II and III, respectively.

Fig. 5 shows the dispersion curves for $2w = 1.1$ mm in this finline geometry. As can be noted, some modal characteristics cross over and the scanned frequency range is large: computing times however are but a fraction of the usual reported in [2] and [6].

If the authors consider the characteristics of the 10th (LSM) and 11th (LSE) modes, reported in Fig. 6, the authors observe that their cutoff frequencies virtually overlap apart for a narrow range near cutoff; the two modes are phase matched over a broad band, while, at the same time, separately carrying active power, being ordinary propagating modes.

Below cutoff, however, *they form a pair of complex modes*; on the other hand, if the fins are removed, these two modes become degenerate. If the authors expand the EM field (6) as a

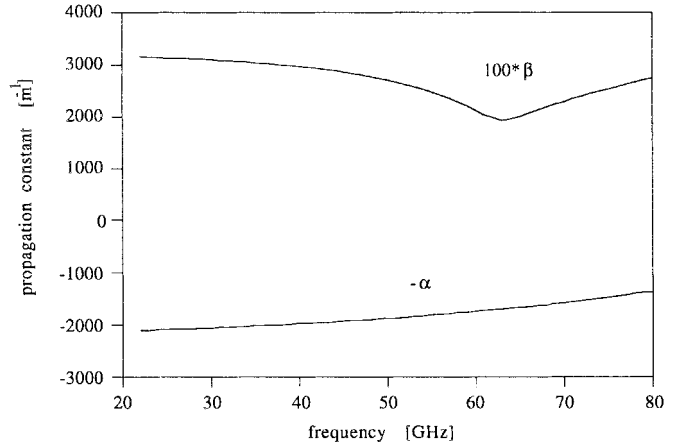

(a)

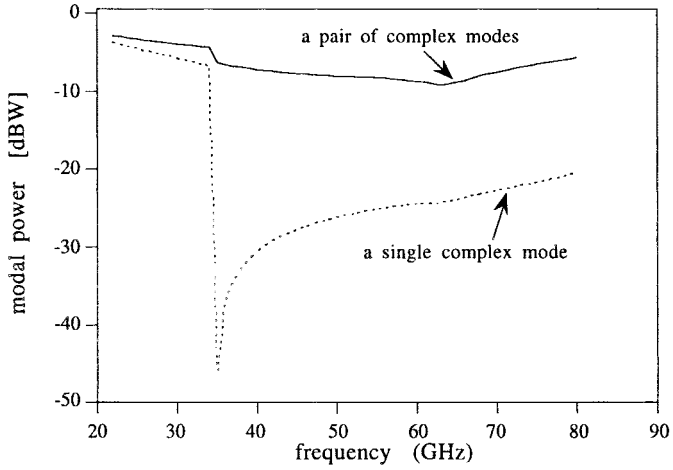

(b)

Fig. 7. (a) Dispersion characteristics of a pair of complex modes for the finline defined in Table II, with $2w = 1.1$ mm. (b) Distribution of the modal power pertaining to the complex modes in (a). Dashed line: power of a single complex mode; continuous line: power of a pair of complex modes.

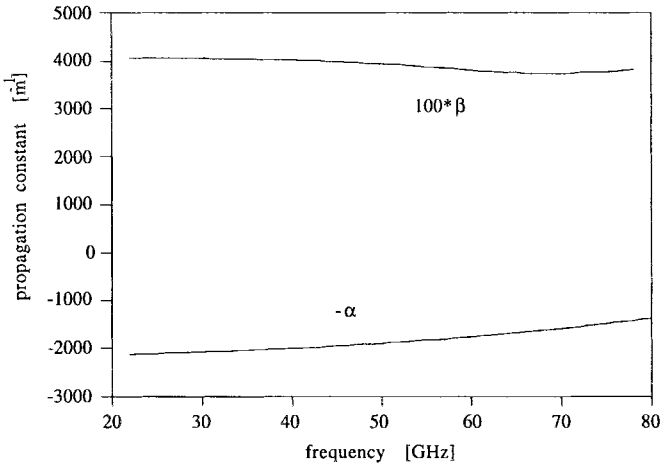

(a)

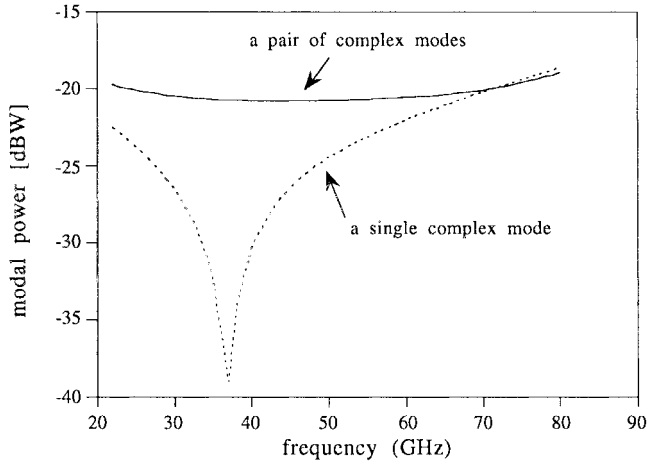

(b)

Fig. 8. (a) Dispersion characteristics of a pair of complex modes for the finline defined in Table II, with $2w = 1.3$ mm. (b) Distribution of the modal power pertaining to the complex modes in (a). Dashed line: power of a single complex mode; continuous line: power of a pair of complex modes.

linear combination of these two modes at cutoff and construct the $\tilde{\mathbf{A}}$, $\tilde{\mathbf{C}}$ matrix (dim 4 × 4), the authors obtain a pair of complex conjugate γ^2 solutions; that is, a two-term expansion is perfectly capable of describing complex characteristics.

In Figs. 7(a) and 8(a) the propagation and attenuation constants of finlines with apertures $2w = 1.1$ mm and $2w = 1.3$ mm, respectively, are reported.

The authors now verify that the power conditions (18) are satisfied by computing

$$P_1 = \iint_S (\mathbf{E}_1 \times \mathbf{H}_1^*) \cdot \mathbf{dS} = \mathbf{I}_1^+ \tilde{\mathbf{A}} \mathbf{V}_1$$

$$P_2 = \iint_S (\mathbf{E}_2 \times \mathbf{H}_2^*) \cdot \mathbf{dS} = \mathbf{I}_2^+ \tilde{\mathbf{A}} \mathbf{V}_2$$

$$P_{12} = \iint_S (\mathbf{E}_1 \times \mathbf{H}_2^*) \cdot \mathbf{dS} = \mathbf{I}_2^+ \tilde{\mathbf{A}} \mathbf{V}_1$$

$$P_{21} = \iint_S (\mathbf{E}_2 \times \mathbf{H}_1^*) \cdot \mathbf{dS} = \mathbf{I}_1^+ \tilde{\mathbf{A}} \mathbf{V}_2.$$

The above quadratic forms are easily calculated, having previously formed the (4 × 4) $\tilde{\mathbf{A}}$ matrix.

P_1 and P_2 represent the power carried by a single complex mode; P_{12} and P_{21} are related to the power carried by a pair of complex modes; namely, the authors have to verify that

$$P_1 = P_2 = 0 \qquad \text{and} \qquad \begin{cases} P_{12} = p \\ P_{12} = -p^* \end{cases} \tag{19}$$

in order to produce a pair of complex modes.

In Fig. 7(b) the modal power distribution corresponding to the complex propagation constant of Fig. 7(a) is shown; the authors observe that the condition (19) is verified over the range 20–80 GHz within the bounds of the discrete truncation error; the computed power carried by a single complex mode is negligible or much less than that carried by a pair of complex modes.

Analogous considerations hold, in the range 30–50 GHz for the finline with $2w = 1.3$ mm, as shown in Fig. 8(b), verifying that the authors are dealing with complex modes.

V. Conclusions

The authors present a theoretically compact and computationally efficient analysis of the propagation of hybrid modes in closed waveguides. Numerical examples were obtained for ordinary and complex propagation of many modes in finline in excellent agreement with existing data.

Due to the explicit formulation of the eigenvalue equation for the complex propagation constant, the proposed method is seen to overcome some of the typical drawbacks of the currently used algorithms, such as low numerical accuracy and efficiency, numerical degeneracy, the appearance of spurious solutions, and the inability of tracing correctly the crossing characteristics of degenerate modes.

This is a prerequisite for evaluating by modal methods discontinuities in planar and other hybrid transmission media by means of small computers.

Appendix

In a lossless reciprocal metal–dielectric guide the electromagnetic (EM) field is hybrid in general, being constituted of coupled LSE and LSM components. For $\omega \neq \omega_t = k_t c$ the authors have

$$\begin{aligned} \mathbf{e}_t(x, y) &= \mathbf{e}_t^{\mathrm{LSE}} + \mathbf{e}_t^{\mathrm{LSM}} \\ \mathbf{h}_t(x, y) &= \mathbf{h}_t^{\mathrm{LSM}} + \mathbf{h}_t^{\mathrm{LSE}}. \end{aligned} \tag{A1}$$

At cutoff ($\omega = \omega_t, \gamma = 0$) the authors obtain the well-known separation of the LSE–LSM components:

$$\begin{aligned} \mathbf{e}_t(x, y) &= \mathbf{e}_t^{\mathrm{LSM}} \\ \mathbf{h}_t(x, y) &= \mathbf{h}_t^{\mathrm{LSE}}. \end{aligned} \tag{A2}$$

The fields in a medium stratified along y can be derived by means of y-directed electric/magnetic Hertzian vector potentials $\overline{\Pi}_e, \overline{\Pi}_h$. Consequently

$$\begin{aligned} \mathbf{E}(x, y, z) &= \nabla\nabla\cdot\overline{\Pi}_e + k^2\overline{\Pi}_e - j\omega\mu\nabla\times\overline{\Pi}_h \\ \mathbf{H}(x, y, z) &= \nabla\nabla\cdot\overline{\Pi}_h + k^2\overline{\Pi}_h + j\omega\varepsilon\nabla\times\overline{\Pi}_e \end{aligned} \tag{A3}$$

where

$$\begin{aligned} \overline{\Pi}_e(x, y, z) &= \Psi_e(x, y)e^{-\gamma z}\hat{\mathbf{y}} \\ \overline{\Pi}_h(x, y, z) &= \Psi_h(x, y)e^{-\gamma z}\hat{\mathbf{y}} \end{aligned} \tag{A4}$$

and propagation has been assumed in the z-direction with propagation constant γ. In (A4) Ψ_e, Ψ_h are the scalar Hertzian potentials, k the wavenumber. The individual field components are given by

$$\begin{aligned} E_x(x, y, z) &= [\partial_x\partial_y\Psi_e(x, y) - j\omega\mu\gamma\Psi_h(x, y)]e^{-\gamma z} \\ E_y(x, y, z) &= [\partial_y^2 + k^2]\Psi_e(x, y)e^{-\gamma z} \\ E_z(x, y, z) &= [-\gamma\partial_y\Psi_e(x, y) - j\omega\mu\partial_x\Psi_h(x, y)]e^{-\gamma z} \end{aligned} \tag{A5a}$$

$$\begin{aligned} H_x(x, y, z) &= [\partial_x\partial_y\Psi_h(x, y) - j\omega\varepsilon\gamma\Psi_e(x, y)]e^{-\gamma z} \\ H_y(x, y, z) &= [\partial_y^2 + k^2]\Psi_h(x, y)e^{-\gamma z} \\ H_z(x, y, z) &= [-\gamma\partial_y\Psi_h(x, y) + j\omega\varepsilon\partial_x\Psi_e(x, y)]e^{-\gamma z}. \end{aligned} \tag{A5b}$$

At the modal cutoff frequencies ($\omega = \omega_t, \gamma = 0$), the above fields reduce to

$$\begin{aligned} e_x(x, y) &= \partial_x\partial_y\Psi_e(x, y) \\ e_y(x, y) &= (\varepsilon_r k_{t_e}^2 + \partial_y^2)\Psi_e(x, y) \Rightarrow \quad \mathbf{e}_t(x, y) = \mathbf{e}_t^{\mathrm{LSM}} \\ e_z(x, y) &= -j\omega\mu\partial_x\Psi_h(x, y) \end{aligned} \tag{A6a}$$

$$\begin{aligned} h_x(x, y) &= \partial_x\partial_y\Psi_h(x, y) \\ h_y(x, y) &= (\varepsilon_r k_{t_h}^2 + \partial_y^2)\Psi_h(x, y) \Rightarrow \quad \mathbf{h}_t(x, y) = \mathbf{h}_t^{\mathrm{LSE}} \\ h_z(x, y) &= j\omega\varepsilon\partial_x\Psi_e(x, y) \end{aligned} \tag{A6b}$$

where $k_{t_{h,e}}$ are cutoff wavenumbers of the LSE/LSM parts of the field, respectively. The potentials Ψ_h, Ψ_e satisfy the following equations

$$(\partial_x^2 + \partial_y^2 + \varepsilon_r k_{t_{h,e}}^2)\Psi_{h,e} = 0. \tag{A7}$$

From (A6) and (A7), the authors can easily show that

$$\nabla_t\cdot\mathbf{e}_t^{\mathrm{LSM}} = 0 \tag{A8a}$$

$$\nabla_t\cdot\mathbf{h}_t^{\mathrm{LSE}} = 0 \tag{A8b}$$

and

$$\nabla_t\left[\frac{1}{k^2}\nabla_t\cdot(h_t^{\mathrm{LSE}}\times\hat{z})\right] = -\frac{k_{th}^2}{k^2}(\mathbf{h}_t^{\mathrm{LSE}}\times\hat{z}) \tag{A9a}$$

$$\nabla_t\left[\frac{1}{k^2}\nabla_t\cdot(\hat{z}\times\mathbf{e}_t^{\mathrm{LSM}})\right] = -\frac{k_{te}^2}{k^2}(\hat{z}\times\mathbf{e}_t^{\mathrm{LSM}}). \tag{A9b}$$

References

[1] T. Itoh, "Spectral domain immittance approach for dispersion characteristics of generalized printed transmission lines," *IEEE Trans. Microwave Theory Tech.*, vol. 28, pp. 733–736, July 1980.

[2] T. Rozzi and C. Railton, "Complex modes in microstrip," *IEEE Trans. Microwave Theory Tech.*, vol. 36, pp. 865–1874, May 1985.

[3] A. M. K. Saad and K. F. Schünemann, "A simple method for analyzing finline structures," *IEEE Trans. Microwave Theory Tech.*, vol. 26, pp. 1002–1011, Dec. 1978.

[4] M. Mrozowski and J. Mazur, "Matrix theory approach to complex waves," *IEEE Trans. Microwave Theory Tech.*, vol. 40, pp. 268–275, Apr. 1992.

[5] Felsen and Marcuvitz, *Radiation and Scattering of Waves.* Englewood Cliffs, NJ: Prentice-Hall, 1973, p. 187.

[6] C. A. Olley and T. Rozzi, "Systematic characterization of the spectrum of unilateral finline," *IEEE Trans. Microwave Theory Tech.*, vol. 34, pp. 1147–1156, Nov. 1986.

[7] A. S. Omar and K. F. Schünemann, "Formulation of the singular integral equation technique for planar transmission line," *IEEE Trans. Microwave Theory Tech.*, vol. 33, pp. 1313–1321.

[8] ———, "Effect of complex modes at finline discontinuities," *IEEE Trans. Microwave Theory Tech.*, vol. 34, pp. 1508–1514, Dec. 1986.

[9] J. Bornemann, "A scattering-type transverse resonance technique for the calculation of (M)MIC transmission line characteristics," *IEEE Trans. Microwave Theory Tech.*, vol. MTT-39, pp. 2083–2088, Dec. 1991.

[10] W.-K. Wang *et al.*, "Investigations of complex modes in a generalized bilateral finline with mounting grooves and finite conductor tickness," *IEEE Trans. Microwave Theory Tech.*, vol. MTT-37, pp. 1891–1897, Dec. 1989.

Tullio Rozzi (M'66–SM'74–F'90) received the "Dottore" degree in physics from the University of Pisa, Italy, in 1965, and the Ph.D. degree in electronic engineering from Leeds University, Leeds, U.K., in 1968. In 1987, he received the D.Sc. degree from the University of Bath, Bath, U.K.

Since 1988, he has been Professor of Antennas in the Department of Electronics and Control (and currently the Head of the department), University of Ancona, Italy, and a Visiting Professor at Bath University. In 1978, he was appointed to the Chair of Electrical Engineering at the University of Liverpool, and in 1981 he was appointed to the Chair of Electronics and Head of the Electronics Group at the University of Bath, where he was Head of the School of Electrical Engineering on an alternate three-year basis. From 1968 to 1978, he was a Research Scientist at the Philips Research Laboratories, Eindhoven, the Netherlands, and in 1975 was a Visiting Researcher at the Antenna Laboratory, University of Illinois, Urbana.

Dr. Rozzi is a Fellow of the IEE and is the IEE Council Representative for Italy. In 1975, he was awarded the Microwave Prize by the IEEE Microwave Theory and Technique Society.

Luca Pierantoni received the "laurea" degree in electronic engineering and the Ph.D. degree in electromagnetic fields, both from the University of Ancona, in 1988 and 1993, respectively.

Since 1989, he has been a Research Fellow at the University of Ancona's Department of Electronics and Automatics. His research interests are in antennas, microwaves, and electromagnetic compatibility.

Marco Farina received the M.Eng. degree (summa cum laude) in electronics and the Ph.D. degree from the University of Ancona, Italy, in 1990 and 1995, respectively.

During 1991–1992, he was Technical Officer in the Italian Army. Since 1992, he has been a Research Fellow with the Department of Electronics and Automatics at the University of Ancona . He is currently with the Institut für Hochfrefrenztechnik, Technical University, Münich, Germany. His research interests are in the analysis and the synthesis of traveling wave amplifiers, the FET mixers design, and the EM modeling of planar devices.